Epithelial Cell Apoptosis Causes Acute Lung Injury Masquerading as Emphysema

Majd Mouded[1], Eduardo E. Egea[1], Matthew J. Brown[1], Shane M. Hanlon[1], A. McGarry Houghton[1], Larry W. Tsai[2], Edward P. Ingenito[2], and Steven D. Shapiro[1]

[1]Division of Pulmonary, Allergy, and Critical Care Medicine, Department of Medicine, University of Pittsburgh School of Medicine, Pittsburgh, Pennsylvania; and [2]Division of Pulmonary and Critical Care Medicine, Brigham and Women's Hospital, Harvard Medical School, Boston, Massachusetts

Theories of emphysema traditionally revolved around proteolytic destruction of extracellular matrix. Models have recently been developed that show airspace enlargement with the induction of pulmonary cell apoptosis. The purpose of this study was to determine the mechanism by which a model of epithelial cell apoptosis caused airspace enlargement. Mice were treated with either intratracheal microcystin (MC) to induce apoptosis, intratracheal porcine pancreatic elastase (PPE), or their respective vehicles. Mice from all groups were inflated and morphometry was measured at various time points. Physiology measurements were performed for airway resistance, tissue elastance, and lung volumes. The groups were further analyzed by air–saline quasistatic measurements, surfactant staining, and surfactant functional studies. Mice treated with MC showed evidence of reversible airspace enlargement. In contrast, PPE-treated mice showed irreversible airspace enlargement. The airspace enlargement in MC-treated mice was associated with an increase in elastic recoil due to an increase in alveolar surface tension. PPE-treated mice showed a loss of lung elastic recoil and normal alveolar surface tension, a pattern more consistent with human emphysema. Airspace enlargement that occurs with the MC model of pulmonary epithelial cell apoptosis displays physiology distinct from human emphysema. Reversibility, restrictive physiology due to changes in surface tension, and alveolar enlargement associated with heterogeneous alveolar collapse are most consistent with a mild acute lung injury. Inflation near total lung capacity gives the appearance of enlarged alveoli as neighboring collapsed alveoli exert tethering forces.

Keywords: apoptosis; emphysema; physiology; murine model

The classic paradigm in emphysema states that progressive alveolar destruction arises from an imbalance between proteases and anti-proteases. In this view chronic inflammation in the lung develops from long-term exposure to inhaled irritants (the most common being cigarette smoke). Inflammatory cells release various proteases, leading to destruction of the extracellular matrix and subsequent loss of the alveolar units.

Recently, however, the role of apoptosis in the pathogenesis of emphysema has become an area of extreme interest. A novel "cell death" hypothesis has been proposed whereby apoptosis of the alveolar cells is believed to be the primary initiator of the disease. This concept arose in part due to the observation that smokers with emphysema have increased alveolar apoptotic cells as compared with smokers without emphysema (1). Subsequent studies demonstrated that experimental induction of either vascular endothelial cell apoptosis or pulmonary epithelial cell apoptosis in animal models results in airspace enlargement (2–5).

Although these apoptotic models replicate some of the morphological changes of human emphysema, they have important differences from more traditional models: (*1*) Only one of the models has reported any increased inflammation (2–5); and (*2*) The airspace enlargement is reversible after withdrawal of the initiating event (2, 5) (although, in fairness, there is a dearth of literature examining this particular issue in the murine smoking model [6]). In addition, previously used epithelial apoptotic insults, such as bleomycin and Fas ligand, have resulted in acute lung injury and fibrosis, but not emphysema (7–10).

To better characterize the pathophysiology of apoptosis-induced airspace enlargement, we compared a destructive, inflammatory model of porcine pancreatic elastase (PPE) to that of an epithelial cell apoptosis model caused by microcystin (MC), a serine/threonine protein phosphatase inhibitor well known to initiate apoptosis (2, 11–14). After treatment with intratracheal instillation of PPE or MC in mice, we examined morphometry and physiology, including measurements of static and dynamic lung elastance, lung volumes, and alveolar surface tension. Our results show that airspace enlargement associated with epithelial cell apoptosis occurs in the setting of a restrictive process caused by increased surface tension resulting from surfactant dysfunction. The increased surface tension appears to cause heterogeneous instability and collapse within the alveolar compartments. This results in adjacent alveolar overdistension due to alveolar–alveolar tethering. We show that the observed airspace enlargement in an alveolar epithelial apoptosis model is mechanistically distinct from the airspace enlargement associated with human emphysema and more traditional elastase animal models.

CLINICAL RELEVANCE

Many believe that structural cell apoptosis is the primary initiator of emphysema. We show that the airspace enlargement in an apoptotic model of emphysema is not consistent with emphysema, but rather reflects acute injury and changes in surface tension.

MATERIALS AND METHODS

Murine Models of Airspace Enlargement

Adult C57Bl/6 female mice (8–10 wk of age; Charles River Laboratories, Wilmington, MA) were used for all experiments. Mice were housed within pathogen-free sterile barrier facilities at the University of Pittsburgh and at Harvard Medical School. The Committee for

(*Received in original form April 8, 2008 and in final form January 8, 2009*)

This work was supported by National Institutes of Health grant R01 HL082541 (S.D.S.).

Correspondence and requests for reprints should be addressed to Steven D. Shapiro, M.D., Division of Pulmonary, Allergy, and Critical Care Medicine, Department of Medicine, University of Pittsburgh School of Medicine, Pittsburgh, PA 15213. E-mail: shapiros@dom.pitt.edu

This article has an online supplement, which is accessible from this issue's table of contents at www.atsjournals.org

Am J Respir Cell Mol Biol Vol 41. pp 407–414, 2009
Originally Published in Press as DOI: 10.1165/rcmb.2008-0137OC on February 2, 2009
Internet address: www.atsjournals.org

Animal Welfare in Research at the University of Pittsburgh and Harvard University approved all animal experiments. Of note, additional experiments using C57BL/6J mice from Jackson Laboratories had identical results (data not shown).

Before instillation of either PPE or MC, to induce airspace enlargement, the mice were anesthetized with an intraperitoneal injection of 2.5% avertin. They were then intubated via direct visualization of the larynx with a 22-gauge intravenous blunt catheter.

Elastase-mediated emphysema was induced by intratracheal administration of 1.5 U PPE (11.1 μg dissolved in 40 μl PBS; Elastin Products, Owensville, MO) and compared with vehicle treatment (40 μl PBS).

Epithelial apoptosis was induced with 2 μg MC (Calbiochem, La Jolla, CA), which was dissolved in sterile 2.5% ethanol. MC and the ethanol vehicle control treatments were administered intratracheally in a total volume of 40 μl.

Tissue Processing

At the completion of each experiment, mice were killed by CO_2 inhalation, the chest was opened, and the right ventricle was perfused with saline. The trachea was cannulated and the lungs were inflated with 10% buffered formalin at 25 cm H_2O pressure for 15 minutes. The lungs were then ligated, removed, and fixed in formalin for 24 hours before embedding in paraffin. Serial midsagittal sections were obtained for morphological and histological analysis.

Morphometry

Midsagittal sections were stained with a modified Gill's stain, and cord lengths were tabulated as previously described (15). A total of 10 randomly selected fields were photographed at ×200 with MetaMorph (Molecular Devices, Sunnyvale, CA). The images were analyzed using Scion Image (Scion Corp., Frederick, MD). Airway and vascular structures were eliminated from the analysis.

Further morphometric analysis was conducted as previously described (16). Briefly, four serial paraffin sections were obtained per animal, and each group of sections being obtained were cut to a depth of 150 μm; 8–10 images (*as described above*) were analyzed per section. Alveoli were identified and tabulated per high-power field, as described (16). All ambiguous structures, airways, and vascular structures were excluded. The tissue and airspace areas (meeting threshold) were tabulated using NIS–Elements BR 3.0 software (Nikon Inc., Tokyo, Japan). Areas were corrected for alveolar number per image. All values were tabulated to determine the means.

Pulmonary Physiology

Physiology measurements, including lung volumes and mechanics, were determined as previously described (17) on groups of mice treated with MC, PPE, or the respective vehicle at predetermined time points corresponding to peak airspace enlargement for each model (MC, 6 hours; PPE, 21 days). Mice were anesthetized with an intraperitoneal injection of 2.5% avertin at doses sufficient to allow spontaneous breathing, yet still provide surgical-concentration anesthesia. A surgical tracheostomy was placed, and lung volumes were measured in triplicate by whole-body plethysmography (BUXCO Systems, Inc., Wilmington, NC). The machine was calibrated before experimentation, and any drift was corrected. FRC was measured by whole-body plethysmography during spontaneous breathing based on Boyle's law (18). Total lung capacity (TLC) was defined as the lung volume at +30 cm H_2O transrespiratory recoil pressure and residual volume as the lung volume measured at −30 cm H_2O transrespiratory recoil pressure. Upon completion of lung volume measurements, additional anesthesia (1/3 original dose) was administered, sufficient to suppress spontaneous respiratory efforts.

The mice were then transferred to a computer-controlled, volume-cycled ventilator (SCIREQ Inc., Montreal, PQ, Canada) for forced oscillatory mechanics measurements to assess airway resistance and dynamic elastance. Mechanical ventilator support was delivered as: f = 150 b/min, V_t = 0.2 ml, 0 positive end-expiratory pressure. Deep inflations to 25 cm H_2O were performed before all measurements to ensure identical volume history profiles. Dynamic lung function (airway resistance, tissue viscosity, and tissue elastance) were assessed in triplicate. Deflation quasistatic pressure–volume profiles (from 30 to 0 cm H_2O distending pressure) were then recorded, and the results fit to the exponential relationship, $V(P) = V_{max} - Ae^{-kP}$, where P is pressure, V_{max} is volume at infinite pressure, A is $V_{max} - V_{min}$, V_{min} is volume at 0 distending pressure, and k is the shape factor that describes the contour of the exponential pressure–volume relationship (19).

Air–Saline Quasistatic Measurements

After physiology measurements, the mice were killed with an intraperitoneal injection of pentobarbital sodium (70 mg/kg), the thorax was opened, and the lungs were degassed by placing the whole mouse in a vacuum chamber. Air–saline quasistatic measurements were then obtained. Briefly, incremental 0.2-ml inflations of air were administered intratracheally while measuring transpulmonary pressure until TLC was reached (transpulmonary pressure = 30 cm H_2O). The lung was then deflated in the same 0.2-ml steps. Pressure measurements were obtained after equilibration of the gas during the deflation limb. The second deflation limb was used for the purposes of analysis to ensure complete recruitment. After air-filled measurements, the lungs were degassed again. The same procedure was repeated, except that the lungs were inflated from 0 vol with room temperature saline. Measurements were made in a similar fashion during deflation. Air and saline-filled deflation quasistatic pressure–volume data were then analyzed by fitting the results to the exponential relationship, $V(P) = V_{max} - Ae^{-kP}$, and summarizing results in terms of V_{max}, A, and k (19).

Bronchoalveolar Lavage Fluid Analysis

At the appropriate time points, subsets of mice were killed and bronchoalveolar lavage (BAL) was performed via a 22-gauge intravenous catheter inserted into the trachea. The lungs were lavaged three times with 1 ml of normal saline each time. The return volume was recorded, and the BAL fluid was centrifuged at 3,000 rpm for 3 minutes to remove cells. The supernatant was set aside for additional analysis, and the cell pellet was treated with hypotonic buffer to lyse red blood cells. The remaining cells were centrifuged at 3,000 rpm for 3 minutes again and resuspended in saline. Total cell counts were determined with a hemocytometer, and differential cell counts determined by manual counting of Geima-stained cytopreps.

Immunohistochemistry: Transferase-Mediated dUTP Nick End Labeling Staining

Immunostaining for surfactant protein (SP) C (goat anti-mouse, 1:500; Santa Cruz Biotechnology, Santa Cruz, CA) and Clara cell 10-kD (CC10) (rabbit anti-mouse, 1:1,000; Millipore, Billerica, MA) proteins was performed. Paraffin-embedded sections were incubated at 60°C for 30 minutes, deparaffinized in xylene, and rehydrated with an ethanol series of washes. Sections were then washed in PBS/0.2% Triton-X100, and blocked for 2 hours with 10% donkey serum in PBS. Primary antibodies were resuspended in the same blocking buffer and incubated overnight at 4°C. The slides were washed in PBS/0.2% Triton-X100 and incubated with either Alexa Flour 488 donkey anti-goat antibody (Invitrogen, Carlsbad, CA) for surfactant staining or Alexa Flour 594 donkey anti-rabbit secondary antibody (Invitrogen) for Clara cell staining for 30 minutes at 37°C. The slides were then washed with PBS and mounted (Vector Laboratories, Burlingame, CA).

Immunstaining for active caspase-3 (rabbit anti-mouse, 1:1,000; Abcam, Cambridge, MA) was performed as stated above, with the exception that an antigen retrieval step was added before permeabilization with 0.2% Triton-X100. For antigen retrieval, slides were incubated in target retrieval solution (Dako, Glostrup, Denmark) per the manufacturer's instructions. The average number of apoptotic cells per high-power field was determined from twenty randomly selected fields (400×) and then corrected for tissue density using the morphometric data as previously described (20).

Transferase-mediated dUTP nick end labeling (TUNEL) staining was performed using the Apoptag kit (Chemicon, Temecula Ca) according to the manufacturer's instructions. The average number of apoptotic cells per high-power field was determined as described above.

Surfactant Assays

After isolation of the cell pellet (*described above*), the remaining BAL fluid was removed and centrifuged at 16,000 × g for 20 minutes to

isolate the surfactant pellet. The pellet was resuspended in 100 μl of 0.02% sodium azide. Phospholipid concentrations were determined by the spectrophotometric method of Stewart (21) referenced to a dipalmitoylphosphatidylcholine standard curve.

Static and dynamic measurements of surface tension of surfactant samples isolated from mouse lungs were performed as previously described (22) with a pulsating bubble surfactometer (Electronetics Corp., Albany, NY). All surfactant samples were prepared at the same final concentration (0.5 mg/ml of total phospholipid) in 2.5 mM $CaCl_2$ solution in 0.9% sodium chloride. A 25- to 30-μl aliquot of sample was loaded into each sample chamber, and air–liquid interface measurements initiated by forming a 0.4-mm diameter. Equilibrium surface tension was measured during static conditions. Minimum surface tension during film compression was recorded during dynamic oscillations performed at 20 cycles/min at 37°C, and atmospheric pressure once samples had come to steady-state conditions (defined as no change in surface tension over a 5-minute period).

Statistical Analysis

Data are presented as mean values (±SEM) unless otherwise indicated. Comparisons between baseline and post-treatment animals for MC-treated, PPE-treated, and vehicle-treated mice at the different time points was performed by single-factor (treatment) one-repeated measures (the outcome variable of interest at different time points) ANOVA for each outcome parameter of interest. Statistical significance was determined by the Student's *t* test (two-tailed distribution with two-sample equal variance). A *P* value less than 0.05 was considered statistically significant.

RESULTS

Airspace Enlargement Is Reversible in an Epithelial Apoptosis Model, whereas It Is Progressive in the Elastase Model

Mice were treated with intratracheal MC, PPE, or their respective vehicles ($n = 8$–10 per group). Maximal airspace enlargement was observed 6 hours after instillation of MC, with resolution (to nonsignificant airspace enlargement relative to control) by 24 hours (Figure 1). PPE-treated mice also developed acute airspace enlargement after instillation; however, it progressed throughout the 21-day study period (Figure 1). BAL was performed to evaluate inflammation. As reported in previous apoptotic models of airspace enlargement, MC did not lead to inflammation, whereas PPE was characterized by acute neutrophilia (Peak Day 1) that gradually resolved, giving way to macrophage accumulation (data not shown) (2–5, 15).

Apoptosis Is a Feature of both Apoptosis and Elastase Models

To lose alveolar units, one would predict that, even in inflammatory models of emphysema, there should be alveolar cell apoptosis. To assess apoptosis in each of these models, tissue sections from MC-, PPE-, and vehicle-treated mice were subjected to TUNEL staining ($n = 8$ per group). TUNEL-positive cells were counted from 20 random fields taken within the lung parenchyma (not central airways and vessels) and corrected for tissue density. The degree of apoptosis after MC administration peaked after 2 hours, as previously described (2). Apoptosis was also observed after PPE administration. The percent of TUNEL-positive cells plateaued in the PPE model between Days 7 and 21 (data not shown). Increased amounts of apoptosis were observed in both models as compared with their respective vehicles (Figures 2A and 2B). As noted in previous studies, the majority of TUNEL-positive cells were alveolar epithelial cells (2, 3, 5) (data not shown). Of note, MC-treated mice had increased peak amounts of apoptosis when compared with the PPE-treated mice.

To further confirm that the cells were apoptotic, staining for active caspase-3 was performed (Figures 2C and 2D) and analyzed as described above. Similar patterns to those of the TUNEL staining were observed with the active caspase-3 staining.

The Apoptosis Model Led to Increased Elastic Recoil in Association with Airspace Enlargement, while Elastase Caused Loss of Elastic Recoil in Association with Airspace Enlargement

To determine the mechanism of airspace enlargement in response to MC and PPE, we performed physiologic measurements by forced oscillatory mechanics and whole-body plethysmography ($n = 14$–18 mice per group for physiology measurements and 12–14 mice per group for lung volume measurements). Dynamic lung physiology was measured at positive end-expiratory pressures of 0 and 5 cm H_20 (to ensure that any derecruitment from anesthesia was overcome). There were no differences in airway resistance measured among the four groups (MC, MC vehicle controls, PPE, and PPE vehicle controls) (Figure 3A). MC-treated mice displayed a physiological pattern distinct from classic emphysema. MC treatment was associated with an increase in dynamic lung elastance, consistent with lung stiffening. PPE treatment was associated with a decrease in dynamic lung elastance, indicating greater lung compliance, a pattern normally observed in emphysema (Figure 3B). Lung volume measurements were consistent with dynamic measurements. MC-treated mice had significant decreases in inspiratory capacity and total lung volume consistent with isopressure reductions in lung volume. PPE-treated mice had increases in functional residual capacity, inspiratory capacity, and total lung volumes, consistent with isopressure increases in lung volume (Figure 3C).

Of note, despite the acute hemorrhage seen with PPE treatment at 6 hours, the measurements of airway resistance and lung elastance were not significantly different from control animals (*see* Figure E1 in the online supplement). This suggests a combined restrictive and obstructive defect that counteracted each other at this early time point.

The Apoptosis Model Was Associated with Increased Surface Tension, Indicating Surfactant Dysfunction

To determine whether the increase in lung elastic recoil associated with MC exposure was due to an increase in tissue recoil or surface tension recoil, we measured air–saline quasi-static pressure–volume curves, as described above ($n = 4$–6 mice per group). MC-treated mice showed a shift in the pressure–volume curve to the right (greater stiffening) when compared with MC vehicle control mice when inflated with air (Figure 4A). There were no differences in pressures when the lungs were filled with saline, indicating that the tissue properties of the lung had not changed after MC treatment. These findings indicate that MC treatment is associated with an isovolume increase in surface tension recoil, but no change in tissue recoil. In the PPE-treated mice, the pressure–volume curves for both the air- and saline-filled lungs shifted to the left (less stiff). The decrease in isovolume pressures in the lungs during both air and saline maneuvers relative to controls indicate that, after PPE treatment, tissue elastic recoil decreases with no change in surface tension recoil (Figure 4B).

Consistent with these findings, immunostaining of MC-treated tissue showed diminished amounts of SPC relative to control (Figure 4C). Of note, PPE-treated mice had decreased tissue density and evidence of emphysema, but did not have an appreciable decrease in SPC by immunohistochemistry. Furthermore, the physiology and chord length resolution that is observed as early as Day 1 is correlated with a return of SPC staining (Figure 4D).

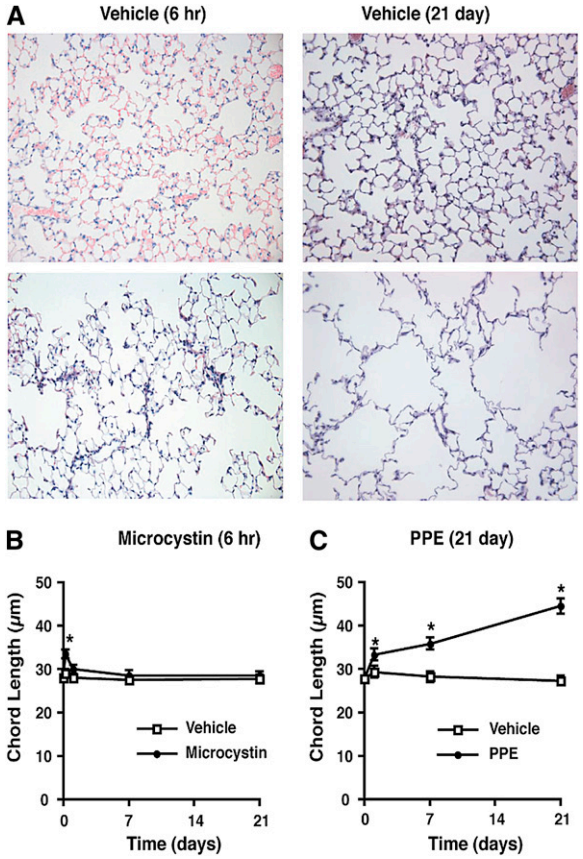

Figure 1. Airspace enlargement in microcystin (MC) and porcine pancreatic elastase (PPE) models. Lungs were fixed in 10% formalin at 25cm H_2O pressure and hematoxylin and eosin–stained midsagittal sections were used to determine chord lengths. (*A*) Representative images of vehicle (MC, *top left*; PPE, *top right*) and maximum airspace enlargement (MC, 6 hours, *bottom left*; PPE, 21 days, *bottom right*). (*B*) Quantification of the average chord lengths of vehicle versus MC is illustrated (*left*), as is that for vehicle versus PPE (*right*). The data are presented as mean values (±SEM). *$P < 0.02$, respective vehicle versus treatment.

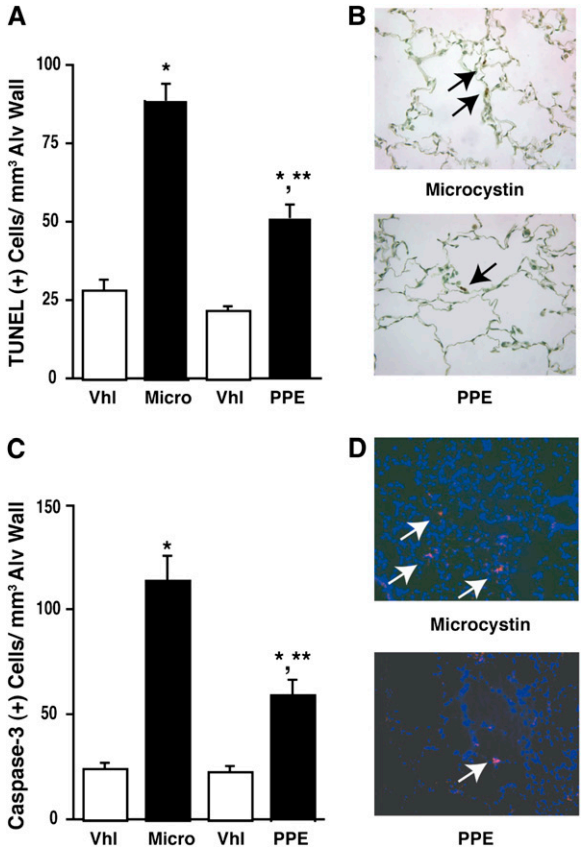

Figure 2. Apoptotic cells after MC and elastase. Lung tissue was stained with transferase-mediated dUTP nick end labeling (TUNEL) to detect DNA cleavage and for active caspase-3 to further confirm apoptosis. Results are shown for peak TUNEL and active caspase-3 positivity in each model (MC, 2 hours; PPE, 21 days). (*A*) Mean number of TUNEL-positive cells were tabulated from 20 random high-power fields. The mean (±SEM) number of positive cells was then corrected for tissue density based on the respective chord lengths. *$P < 0.01$ compared with the respective vehicles; **$P < 0.02$ MC versus PPE. (*B*) Representative images of TUNEL-positive cells are shown (*arrows*) for MC (*top*) and PPE (*bottom*). Note that TUNEL positivity counterstained with diaminobenzidine (DAB) appear as *brown*. The remaining tissue is counterstained with methyl green. (*C*) Mean number of active caspase-3–positive cells was tabulated from 20 random high-power fields. The values are presented as the mean (±SEM) number of positive cells corrected for tissue density, as described above. (*D*) Representative images of active caspase-3–positive cells are shown (*arrows*) for MC (*top*) and PPE (*bottom*). Active caspase-3 appears as *red*. Nuclear counterstaining with 4′,6′-diamidino-2-phenylindole (DAPI) appears as *blue*.

Direct measurements of the interfacial properties of lung surfactant isolated from MC- and PPE-treated mice support the conclusions of air- and liquid-filled quasistatic lung physiology. Both vehicle control groups and PPE-treated mice all had similar surfactant function. MC-treated mice had decreased surfactant function, with elevations in both static and dynamic surface tension measurements (Table 1). Together, these data suggest that the increased lung elastance and decreased isopressure lung volumes observed after MC are due to alterations in surfactant function secondary to MC-induced injury.

Variable Volume Lung Inflations Demonstrate Acute Lung Injury and Alveolar Collapse as the Basis for Airspace Enlargement in the Apoptosis Model

Results summarized above suggest that MC treatment is associated with an increase in lung elastance due to surfactant dysfunction. PPE treatment is associated with a decrease in lung elastance due to tissue destruction. To assess whether surfactant dysfunction and alveolar destabilization could result in overdistention of remaining patent alveoli after MC treatment, we subjected our samples to further morphometric analysis. To confirm this mechanism, we fixed MC-treated lungs at sub-TLC isovolumes to further exacerbate this finding.

Block sections were obtained from each group ($n = 5$ animals per group) at peak airspace enlargement (6 hours for MC animals and 21 days for PPE-treated animals) to calculate alveolar number, tissue areas, alveolar areas, and alveolar numbers. As expected, the number of alveoli (alveoli per high-power field) per lung decreased in both groups (Figure 5A). With the increased alveolar size, there was a trend for an increase in tissue area per alveolus in the PPE group, and a significant increase in tissue area per alveolus in the MC group (Figure 5B). Both treatment groups, in concordance with their increased chord lengths, showed an increase in the alveolar area per alveolus (Figure 5C). If collapsed alveoli contribute to a decreased amount of patent alveoli with overdistention of nearby alveoli, then one would expect the amount of tissue relative to alveolar enlargement to increase. This is in direct contrast to true emphysema, where tissue

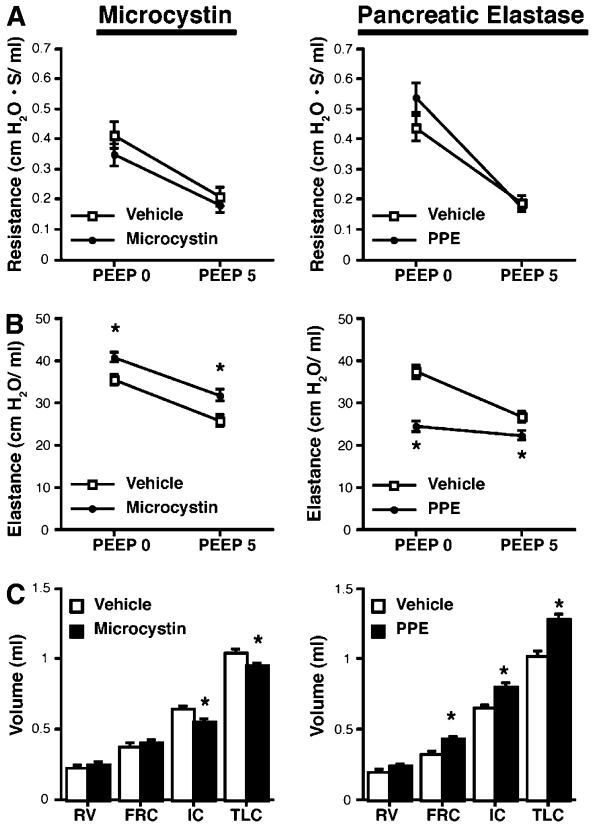

Figure 3. Physiology in apoptosis and elastase-induced airspace enlargement. Physiology measurements were performed on all four treatment groups during time points of peak airspace enlargement (6 hours for MC experiments; 21 days for PPE experiments). Airway resistance and tissue elastance were measured at positive end-expiratory pressure (PEEP) 0 and 5 cm H_2O with a flexiVent ventilator. Lung volumes and lung capacities were measured with a Buxco plethysmography box. (*A*) Measurements of airway resistance, vehicle versus MC (*left*), and vehicle versus PPE (*right*). (*B*) Measurements of tissue elastance: vehicle versus MC (*left*) and vehicle versus PPE (*right*). (*C*) Measurements of residual volume (RV), functional residual capacity (FRC), inspiratory capacity (IC), and total lung capacity (TLC), vehicle versus MC (*left*) and vehicle versus PPE (*right*). The data are presented as mean values (±SEM). *$P < 0.02$, vehicle versus treatment.

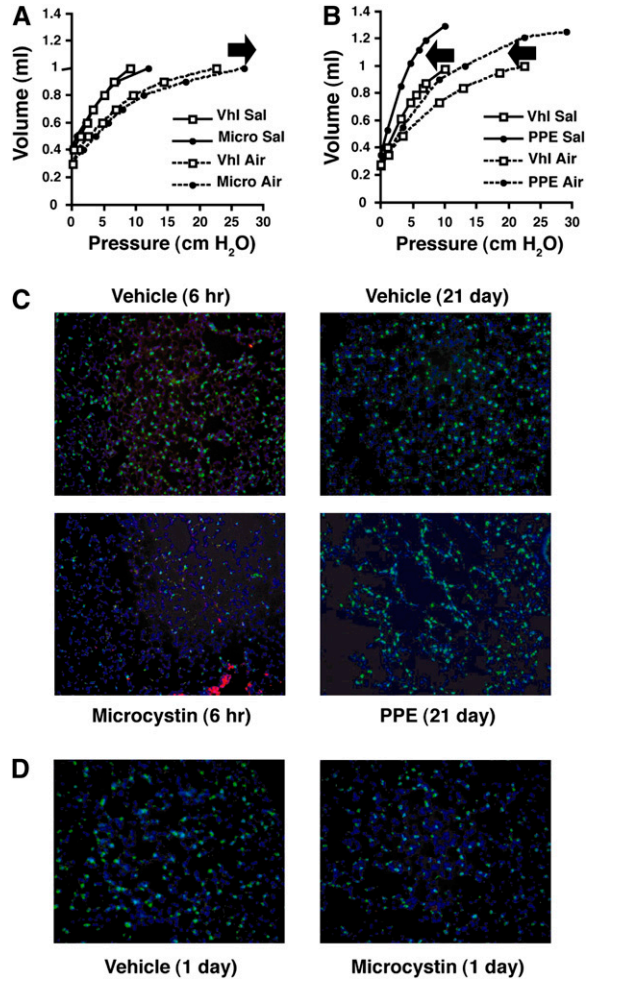

Figure 4. Air–saline quasistatic pressure–volume curves and surfactant protein (SP) C immunostaining. To determine the contribution of surface tension to the changes in tissue elastance, air–saline quasistatic pressure–volume measurements were taken on mice treated with vehicle or MC at peak airspace size (6 hours) and on mice treated with vehicle or PPE at peak airspace size (21 days). Open chest degassed lungs were inflated with fixed volumes of air, followed by repeat degassing, saline washout, and fixed-volume saline inflations. Pressures were measured during deflation at each lung volume, and a curve fit was generated. Variation in pressures measured between air and saline inflations reflects the contribution of surface tension to the change in elastance of the lung. (*A*) Graphing of air–saline quasistatic pressure–volume curves for vehicle versus MC. *Arrows* illustrate the curve shift(s) for treatment compared against vehicle. (*B*) Graphing of air–saline quasistatic pressure–volume curves for vehicle versus PPE. (*C*) Immunostaining of lung tissue for SPC and Clara cell 10 kD protein (CC-10) was performed. SPC appears as *green*, CC-10 appears as *red*, and nuclear counterstaining with DAPI appears as *blue*. Representative images at these time points are shown from vehicle (*top left*) versus MC-treated lungs (*bottom left*), and PPE vehicle (*top right*) versus PPE-treated lungs (*bottom right*). (*D*) By Day 1, physiology and morphometry of MC-treated animals began to normalize, which correlates with a return of surfactant. Representative images for SPC staining, performed as described above, at Day 1 are shown for vehicle (*left*) and MC-treated animals (*right*).

destruction would lead to a relative decrease in the amount of tissue relative to the alveolar size. To determine this, in our study, the ratio of tissue area to alveolar area was determined. This ratio, as expected, showed a relative decrease in the amount of tissue as the alveolar size increased in the PPE group compared with the vehicles. The MC group showed a relative increase in the amount of tissue as the alveolar area increased compared with both vehicles and PPE, implying areas of collapsed alveoli (Figure 5D).

To further analyze if collapsed alveoli could lead to overdistention of the surrounding alveoli, we performed fixed-volume inflations. By keeping inflation volume constant, variable intra-alveolar pressures would be generated, depending on lung elastance/compliance. Results of the air–saline quasistatic pressure–volume data from Figure 4A are represented differently in Figure 5E by subtracting isovolume saline-filled recoil pressures (representing elastic recoil pressure of the lung tissue) from air recoil pressures (representing both the tissue properties of the lung and pressure due to surface tension) to allow calculation of the percent recoil contributed by surface tension at each volume.

Figure 5 shows that, in MC-treated animals, as lung volumes increase, the contribution from surface tension to the recoil of the lung decreases. To augment the effects of surface tension after MC (6 hours), we inflated the lungs to approximately 50% TLC with a fixed 0.5-ml volume of 10% buffered formalin (volumes

TABLE 1. SURFACE TENSION MEASUREMENTS AT PEAK AIRSPACE ENLARGEMENT

BAL Sample	Surface Tension, Static (*dyn/s*)	Surface Tension, Dynamic (*dyn/s*)
MC vehicle	22.92 ± 0.52	6.58 ± 1.42
MC	26.95 ± 0.54*	18.28 ± 1.56*
PPE vehicle	23.36 ± 0.58	7.64 ± 0.75
PPE	23.67 ± 0.71	7.10 ± 0.94

Definition of abbreviation: MC, microcystin; PPE, porcine pancreatic elastase.

Direct measurement of surfactant function was performed with a surfactometer. Vehicle and MC–treated animals were lavaged at peak airspace enlargement (6 hours), and vehicle and PPE–treated animals were lavaged at 21 days. The samples were normalized for phospholipid concentrations. Surface tension was measured before and after 20 minutes of agitation. Data are presented as mean values (±SEM).

* $P < 0.01$.

determined from plethysmography from Figure 3C). The representative images show diffusely underinflated lungs in the vehicle control group. In the MC group, however, there are areas with complete collapse of the alveoli with overdistension of adjoining alveoli (Figure 5F). The overdistended alveoli in this setting do not represent emphysema, as they are not generated by cleavage of the extracellular matrix and loss of functional alveoli.

DISCUSSION

This study demonstrates that the mechanism of airspace enlargement after alveolar epithelial cell apoptosis associated with MC administration is fundamentally different from that associated with PPE treatment. After intratracheal PPE instillation, we observed progressive, irreversible airspace enlargement with loss of lung elastic recoil and evidence of isopressure airspace enlargement relative to control animals. By contrast, intratracheal instillation of MC caused epithelial cell apoptosis, with an increase in lung elastic recoil and transient airspace enlargement due to surfactant dysfunction, heterogeneous airspace collapse, and overdistention of adjacent patent alveoli due to tethering. Morphology of MC-treated lungs examined at sub-TLC volumes suggests that the pattern of alveolar tethering and overdistention due to surfactant dysfunction can be confused with emphysema if studies are limited to lung volumes near TLC.

Traditionally, the pathophysiology of emphysema has been attributed to progressive destruction of the extracellular matrix by inflammatory cell proteinases, particularly elastases, as a result of long-standing inflammation. Tissue destruction results in progressive airspace enlargement accompanied by loss of tissue recoil. The notion that apoptosis is an important primary event in the pathogenesis of emphysema represents a major recent paradigm shift. The apoptosis hypothesis proposes that alveolar septal cell apoptosis is the first step in the process, leading to

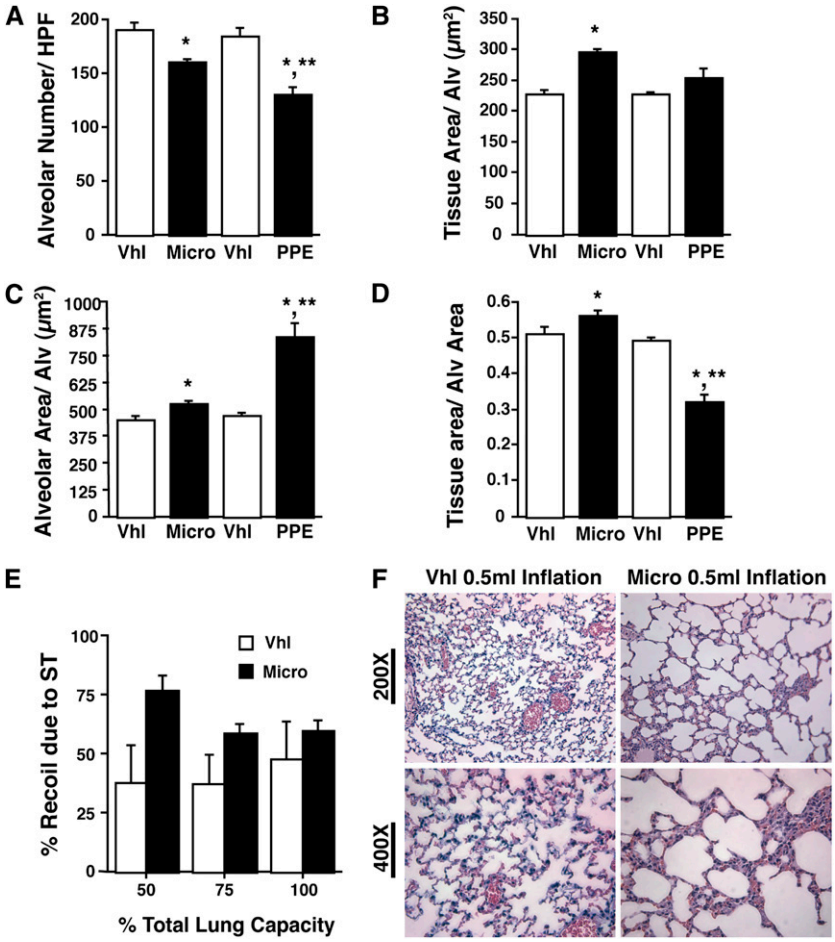

Figure 5. Analysis of tissue area and alveolar areas, and the effects of variable volume inflation on surface tension and airspace enlargement. Further analysis of whole lung tissue was as described in MATERIALS AND METHODS. Alveolar number, tissue areas, alveolar areas, and alveolar numbers were tabulated from five animals per group at peak airspace enlargement for both groups (6 hours for MC-treated animals; 21 days for PPE-treated animals). Four block sections from both lungs were taken, and 8–10 images per section were analyzed. Tissue area and alveolar area were normalized for alveolar number. A ratio of tissue area per alveolus versus alveolar area per alveolus was determined for each section and averaged. (*A*) Alveolar numbers (shown as mean per high-power field) reveal a decrease in the number of alveoli in both treatment groups, with PPE-treated animals having a further decrease in the number of alveoli. (*B*) Tissue area per alveolus quantification shows an increased tissue area per alveolus for MC-treated animals as compared with other groups. (*C*) As seen with the cord lengths, alveolar area for both MC-treated and PPE-treated animals, with PPE-treated animals showing even further increases in alveolar area/alveolus. (*D*) The ratio of tissue area/alveolus to alveolar area/alveolus shows an increase in the amount of tissue corrected for airspace enlargement in the MC-treated animals. The converse is true for the PPE-treated animals, with less tissue present when corrected for alveolar area. Values are mean values (±SEM). *$P < 0.05$ compared with the respective vehicles; **$P < 0.01$ MC versus PPE. Furthermore, to better understand and demonstrate how variable pressures generated from changes in surface tension in the MC models could lead to airspace enlargement, the lungs were inflated with a fixed volume of 10% buffered formalin. (*E*) Quantification of relative contribution of surface tension determined by the difference in deflation pressures between air- and saline-filled lungs was graphed. The pressure values were taken from Figure 4A. The quantification demonstrated a larger contribution of pressure due to surface tension at lower lung volumes in the MC model as compared with larger lung volumes. (*F*) Fixed-volume inflations with 0.5 ml (~50% TLC) were performed. Representative images of the affected areas are shown for vehicle at 200× (*top left*) and for a closer view at 400× (*bottom left*), and MC at 200× (*top right*) and again at 400× (*bottom right*).

loss of tissue mass and airspace enlargement. In support of this concept, inhibition of vascular endothelial growth factor (VEGF) receptor-2 has been shown to cause alveolar endothelial cell apoptosis, pruning of the pulmonary arterial tree, and airspace enlargement in rats (3). Emphysema in this model could be prevented by treatment with the caspase inhibitor, Z-Asp-CH_2-DCB. Ceremide also was shown to cause endothelial cell death–mediated emphysema (4). Targeting of primarily epithelial cell death, using mediators such as caspase-3 and nodularin/MC, also resulted in airspace enlargement (2, 4).

Although emphysema is defined pathologically as airspace enlargement, there is little evidence that the physiology of experimental apoptosis models of emphysema resembles the physiology of human emphysema. Lung physiology performed previously by investigators working with the intratracheal VEGF*lox*P/adenoviral cyclization recombinase (CRE) apoptotic model, showed a decrease in elastance in the treated animals (5). However, the abnormally low values of TLC reported in this study for control C57Bl/6 mice (23) at a transpulmonary pressure of 30 cm H_2O raises concerns about the adequacy of these measurements (i.e., both controls and treatment group appeared to have abnormal restrictive physiology). Strikingly, in our study, we observed increased elastance in the epithelial cell apoptotic model, as opposed to the decreased lung elastance that is characteristic of pulmonary emphysema. The two determinants of total lung recoil are tissue recoil and surface tension recoil. To determine the basis for increased lung elastance in the apoptotic model, we performed air–saline quasistatic pressure–volume measurements. In an open-chest animal, when the lungs are filled with air, the pressures measured at the airway opening are due both to tissue and surface film recoil. When the lungs are fully degassed and filled with saline, pressure is determined solely by tissue recoil. Based upon air–liquid–filled deflation pressure–volume data, we determined that MC-treated mice have increased surface tension recoil, but normal tissue recoil. The increase in total lung recoil is therefore due to an increase in surface tension recoil associated with MC treatment. Elastase-treated animals, however, showed decreases in total lung elastic recoil, associated with a loss of tissue recoil, but normal surface tension recoil. Surfactant protein immunostaining and functional studies confirmed that surfactant dysfunction was responsible for the increased surface tension in the apoptotic model. Furthermore, the normalization of chord length and physiology was associated with the return of surfactant.

We postulate that increases in surface tension can result in airspace enlargement by causing heterogeneous alveolar instability, collapse, and distention of patent nearby alveoli (24). Mild, heterogeneous lung injury can result in areas that collapse at lower volumes. These alveoli exert distending pressure on the surrounding alveoli. At very high distending pressures, many of the collapsed alveoli may, in fact, be recruited, making the findings of alveolar collapse and surrounding overdistention very subtle. Alveolar collapse and the tethering open of adjacent alveoli in the epithelial apoptosis model can be deduced from morphometric determination of tissue area ratios to alveolar area ratios. MC results in more tissue per unit of airspace enlargement (a larger tissue area:alveolar area ratio), whereas elastase shows just the opposite. This phenomenon can be more easily visualized by inflation at sub-TLC volumes (Figure 5).

Repair in emphysema is believed to be limited due to the loss of the elastic cable matrix structure. Reinitiation of elastic fiber assembly requires a complex series of events. Tropoelastin must be produced and chaperoned to the cell surface, where it binds to a microfibrillar scaffold composed of several proteins, including fibrillins, microfibril-associated proteins, latent transforming growth factor binding proteins, fibulin, and potentially others. Tropoelastin is then cross-linked by lysyl oxidase. It is likely that spatial and temporal coordination of these events is limited in adults, explaining irreversibility of emphysema. In the cell death–initiated models, lack of inflammation and intact extracellular matrix (data not shown) would explain the ability to replenish lost cells and produce functional surfactant. In fact, the tissue physiology returns back to baseline within 1–3 days of exposure in this model. As with other forms of acute lung injury, particularly in the absence of inflammation, if limited to cellular injury with an intact matrix, there is the capacity for full restoration of alveolar architecture.

Epithelial cell apoptosis is a prominent feature, and, in fact, the inciting event in several models of acute lung injury and pulmonary fibrosis, including the classic bleomycin model (9), as well as Fas ligand–mediated acute respiratory distress syndrome (8, 10). Indeed, it seems likely that all models of epithelial cell apoptosis lead to acute lung injury. Perhaps single administration of epithelial apoptotic agents lead to a mild, heterogeneous, and noninflammatory acute lung injury, whereas repeated acute insults may ultimately lead to an inflammatory cascade resulting in permanent airspace enlargement and emphysema.

Of note, this study was limited to administration of a single apoptotic agent administered intratracheally to lung epithelial cells. Primary endothelial cell apoptosis may, in fact, be more closely akin to what might occur in emphysema. However, airspace enlargement with these endothelial cell–specific agents has been quite mild (3) and reversible. Luckily, VEGF receptor-2 inhibitors have been used as therapeutics for patients with lung cancer for several years, without reports of emphysema. Further physiologic testing in these models, as well as the cigarette smoking model, is also warranted. Indeed, a major point here is that one must fully characterize all animal models to fully understand their relevance to human disease.

This study is not meant to deemphasize the potential importance of apoptosis in the pathophysiology of emphysema. Loss of an alveolar unit by any means must involve loss of both extracellular matrix and cells. Hence, apoptosis clearly occurs in chronic obstructive pulmonary disease and has important physiologic consequences. Uptake of apoptotic cells by macrophages leads to production of antiinflammatory factors, such as transforming growth factor -β, and growth factors, such as human growth factor (25–28). Hence, apoptosis might limit lung injury and promote repair. In contrast, overwhelming cell death or defective clearance mechanisms may lead to secondary necrosis and become proinflammatory.

The question remains whether apoptosis is a primary event leading to emphysema, or whether it is secondary to extracellular matrix destruction followed by loss of cellular attachment and, hence, cell death, a condition termed anoikis. We observed apoptosis in both the MC as well as the PPE model. Apoptosis has also been observed in humans with chronic obstructive pulmonary disease (1). The data presented here suggest, however, that epithelial cell apoptosis may not be the primary event that leads to emphysema. Rather, our results suggest that this is a secondary event, and that protease-based experimental models of emphysema most closely resemble human emphysema.

Conflict of Interest Statement: None of the authors has a financial relationship with a commercial entity that has an interest in the subject of this manuscript.

References

1. Kasahara Y, Tuder RM, Cool CD, Lynch DA, Flores SC, Voelkel NF. Endothelial cell death and decreased expression of vascular endothe-

lial growth factor and vascular endothelial growth factor receptor 2 in emphysema. *Am J Respir Crit Care Med* 2001;163:737–744.
2. Aoshiba K, Yokohori N, Nagai A. Alveolar wall apoptosis causes lung destruction and emphysematous changes. *Am J Respir Cell Mol Biol* 2003;28:555–562.
3. Kasahara Y, Tuder RM, Taraseviciene-Stewart L, Le Cras TD, Abman S, Hirth PK, Waltenberger J, Voelkel NF. Inhibition of VEGF receptors causes lung cell apoptosis and emphysema. *J Clin Invest* 2000;106:1311–1319.
4. Petrache I, Natarajan V, Zhen L, Medler TR, Richter AT, Cho C, Hubbard WC, Berdyshev EV, Tuder RM. Ceramide upregulation causes pulmonary cell apoptosis and emphysema-like disease in mice. *Nat Med* 2005;11:491–498.
5. Tang K, Rossiter HB, Wagner PD, Breen EC. Lung-targeted VEGF inactivation leads to an emphysema phenotype in mice. *J Appl Physiol* 2004;97:1559–1566. (discussion, p. 1549).
6. Martin RL, Shapiro SD, Tong SE, Van Wart H. Macrophage metalloelastase inhibitors. In: Hansel TT, Barnes PJ, editors, Progress in respiratory research. Vol. 31, New drugs for asthma, allergy and COPD. Basel: Karger; 2001. pp. 177–180.
7. Budinger GR, Mutlu GM, Eisenbart J, Fuller AC, Bellmeyer AA, Baker CM, Wilson M, Ridge K, Barrett TA, Lee VY, *et al.* Proapoptotic bid is required for pulmonary fibrosis. *Proc Natl Acad Sci USA* 2006;103: 4604–4609.
8. Hagimoto N, Kuwano K, Miyazaki H, Kunitake R, Fujita M, Kawasaki M, Kaneko Y, Hara N. Induction of apoptosis and pulmonary fibrosis in mice in response to ligation of Fas antigen. *Am J Respir Cell Mol Biol* 1997;17:272–278.
9. Chua F, Gauldie J, Laurent GJ. Pulmonary fibrosis: searching for model answers. *Am J Respir Cell Mol Biol* 2005;33:9–13.
10. Matute-Bello G, Wurfel MM, Lee JS, Park DR, Frevert CW, Madtes DK, Shapiro SD, Martin TR. Essential role of MMP-12 in Fas-induced lung fibrosis. *Am J Respir Cell Mol Biol* 2007;37:210–221.
11. Chen T, Wang Q, Cui J, Yang W, Shi Q, Hua Z, Ji J, Shen P. Induction of apoptosis in mouse liver by microcystin-LR: a combined transcriptomic, proteomic, and simulation strategy. *Mol Cell Proteomics* 2005;4:958–974.
12. Fladmark KE, Brustugun OT, Mellgren G, Krakstad C, Boe R, Vintermyr OK, Schulman H, Doskeland SO. Ca^{2+}/calmodulin-dependent protein kinase ii is required for microcystin-induced apoptosis. *J Biol Chem* 2002;277:2804–2811.
13. Fu W-y, Chen J-p, Wang X-m, Xu L-h. Altered expression of p53, Bcl-2 and Bax induced by microcystin-LR *in vivo* and *in vitro. Toxicon* 2005;46:171–177.
14. McDermott CM, Nho CW, Howard W, Holton B. The cyanobacterial toxin, microcystin-LR, can induce apoptosis in a variety of cell types. *Toxicon* 1998;36:1981–1996.
15. Houghton AM, Quintero PA, Perkins DL, Kobayashi DK, Kelley DG, Marconcini LA, Mecham RP, Senior RM, Shapiro SD. Elastin fragments drive disease progression in a murine model of emphysema. *J Clin Invest* 2006;116:753–759.
16. Massaro GD, Massaro D. Postnatal treatment with retinoic acid increases the number of pulmonary alveoli in rats. *Am J Physiol* 1996;270:L305–L310.
17. Simon DM, Arikan MC, Srisuma S, Bhattacharya S, Tsai LW, Ingenito EP, Gonzalez F, Shapiro SD, Mariani TJ. Epithelial cell PPAR[gamma] contributes to normal lung maturation. *FASEB J* 2006;20:1507–1509.
18. Ingenito EP, Reilly JJ, Mentzer SJ, Swanson SJ, Vin R, Keuhn H, Berger RL, Hoffman A. Bronchoscopic volume reduction: a safe and effective alternative to surgical therapy for emphysema. *Am J Respir Crit Care Med* 2001;164:295–301.
19. Salazar E, Knowles JH. An analysis of pressure volume characteristics of the lungs. *J Appl Physiol* 1964;19:97–104.
20. Maeno T, Houghton AM, Quintero PA, Grumelli S, Owen CA, Shapiro SD. $Cd8^+$ T cells are required for inflammation and destruction in cigarette smoke–induced emphysema in mice. *J Immunol* 2007;178: 8090–8096.
21. Stewart JC. Colorimetric determination of phospholipids with ammonium ferrothiocyanate. *Anal Biochem* 1980;104:10–14.
22. Ingenito EP, Mora R, Cullivan M, Marzan Y, Haley K, Mark L, Sonna LA. Decreased surfactant protein-B expression and surfactant dysfunction in a murine model of acute lung injury. *Am J Respir Cell Mol Biol* 2001;25:35–44.
23. Tankersley CG, Rabold R, Mitzner W. Differential lung mechanics are genetically determined in inbred murine strains. *J Appl Physiol* 1999; 86:1764–1769.
24. Wiebel E. Section 3: the respiratory system. Handbook of physiology. Mechanics of breathing. Bethesda: American Physiologic Society; 1986.
25. Fadok VA, Bratton DL, Guthrie L, Henson PM. Differential effects of apoptotic versus lysed cells on macrophage production of cytokines: role of proteases. *J Immunol* 2001;166:6847–6854.
26. Fadok VA, Bratton DL, Konowal A, Freed PW, Westcott JY, Henson PM. Macrophages that have ingested apoptotic cells *in vitro* inhibit proinflammatory cytokine production through autocrine/paracrine mechanisms involving TGF-beta, PGE2, and PAF. *J Clin Invest* 1998;101:890–898.
27. Henson PM, Cosgrove GP, Vandivier RW. State of the art: apoptosis and cell homeostasis in chronic obstructive pulmonary disease. *Proc Am Thorac Soc* 2006;3:512–516.
28. Huynh ML, Fadok VA, Henson PM. Phosphatidylserine-dependent ingestion of apoptotic cells promotes TGF-beta1 secretion and the resolution of inflammation. *J Clin Invest* 2002;109:41–50.